Field evaluation of a low-powered, profiling $p\mathrm{CO_2}$ system in coastal Washington

Sophie N. Chu [iD],[1,2]* Adrienne J. Sutton,[2] Simone R. Alin,[2] Noah Lawrence-Slavas,[2] Dariia Atamanchuk,[3] John B. Mickett,[4] Jan A. Newton,[4] Christian Meinig,[2] Scott Stalin,[2] Anders Tengberg[5,6]

[1]Joint Institute for the Study of the Atmosphere and Ocean, University of Washington, Seattle, Washington, USA
[2]Pacific Marine Environmental Laboratory, National Oceanic and Atmospheric Administration, Seattle, Washington, USA
[3]Department of Oceanography, Dalhousie University, Halifax, Nova Scotia, Canada
[4]Applied Physics Laboratory, University of Washington, Seattle, Washington, USA
[5]Department of Marine Sciences, University of Gothenburg, Gothenburg, Sweden
[6]Aanderaa Data Instruments AS, Bergen, Norway

Abstract

Summertime upwelling of deep, corrosive waters on the continental shelf of the northern California Current System can exacerbate ocean acidification conditions, providing unsuitable environments for development of calcifying organisms and finfish that are important to the local economy. To better understand the carbonate system in this dynamic region, two recently developed technologies were combined with other sensors to obtain high-frequency carbon profile data from July 2017 to September 2017. The compact, low-power sensor package was composed of an optical sensor for partial pressure of carbon dioxide ($p\mathrm{CO_2}$ optode, Aanderaa model #4797) integrated onto a wave-powered PRofiling crAWLER (PRAWLER). The PRAWLER profiled from 3 to 80 m, stopping at fixed depths for varying lengths of time to allow for $p\mathrm{CO_2}$ equilibration. $p\mathrm{CO_2}$ derived from a regional empirical algorithm was used to correct optode drift using data at 80 m. Near-surface adjusted optode $p\mathrm{CO_2}$ agreed within $6 \pm 42\ \mu$atm to surface $p\mathrm{CO_2}$ from a nearby Moored Autonomous $p\mathrm{CO_2}$ instrument. Throughout the water column, optode $p\mathrm{CO_2}$ compared to algorithm $p\mathrm{CO_2}$ within $-28 \pm 66\ \mu$atm. Overall, optode uncertainty was 35–72 μatm based on root-mean-square errors from all comparison data sets. Errors are attributed to optode calibration, adjustment, algorithm uncertainty, and environmental variability between optode and reference data. Improvements for optode performance within this profiling application include using more stable sensing foils, in situ calibration, and pumped flow over the sensing foil. Additionally, the study revealed undersaturated (corrosive) waters with respect to aragonite below 60 m throughout the deployment that reached up to 40 m by mid-September.

Over the last 250 yr, anthropogenic carbon dioxide ($\mathrm{CO_2}$) absorbed by the surface ocean has led to a measurable decrease in pH, or increase in acidity, in a process known as ocean acidification (OA) (Caldeira and Wickett 2003; Feely et al. 2004; Orr et al. 2005; Doney et al. 2009). During this time, surface pH in the open ocean has decreased by ~ 0.11 pH units and is expected to decrease by another 0.3–0.4 units before the end of the century (Orr et al. 2005). OA causes a decrease in carbonate ion concentration and calcium carbonate saturation states, which directly affects the ability of calcifying marine organisms to build their shells and skeletons (Feely et al. 2004).

On local scales and particularly in the coastal ocean, it is challenging to quantify OA and its effects on marine ecosystems due to large variability of natural and anthropogenic physical and biogeochemical processes (Bauer et al. 2013). Coastal regions that experience upwelling may be particularly vulnerable to intensified OA because of the especially high $\mathrm{CO_2}$ in upwelled waters compared to background values (Feely et al. 2008, 2016a, 2018; Fassbender et al. 2011; Harris et al. 2013). Because of high rates of respiration, which increases $\mathrm{CO_2}$ and decreases pH and dissolved oxygen ($\mathrm{O_2}$), the deep, upwelled waters expose organisms to multiple stresses from both OA and hypoxia (Chan et al. 2008; Reum et al. 2015; Siedlecki et al. 2016). Additionally, nutrient runoff into coastal waters can exacerbate stress from natural variability, causing enhanced eutrophication and even stronger effects from hypoxia and OA (Cai et al. 2011; Wallace et al. 2014).

*Correspondence: sochu@uw.edu

Despite its importance to the economy and ecology that society values, the coastal ocean remains largely undersampled considering its high variability through space and time. In order to study dynamics of the carbonate system in the coastal ocean, in situ sensors are needed to provide accurate, high-resolution measurements of inorganic carbon parameters and pH. Traditional shipboard samples only provide snapshots of the state of the carbonate system. With autonomous, in situ platforms and sensors, spatially and temporally resolved carbon data will enable us to better assess and understand OA in the coastal ocean, at the convergence of processes such as eutrophication, upwelling, and respiration.

Over the past decade, there have been many improvements to technologies that measure the seawater carbonate system to help quantify OA. The seawater carbonate system can be fully characterized by measuring or estimating two of the four following parameters: pH, partial pressure of CO$_2$ (pCO$_2$), total alkalinity (TA), and dissolved inorganic carbon (DIC). pCO$_2$ and pH autonomous sensor technologies are relatively mature (DeGrandpre et al. 1995; Seidel et al. 2008; Martz et al. 2010, 2015; Sutton et al. 2014); however, they are often restricted to surface platforms with an infrastructure that can accommodate the sensors' typically large physical size and significant power and reagent requirements. Thus, there is a need for more compact and low-power full-depth technologies that are still capable of maintaining climate-quality standards of measurement uncertainty (Newton et al. 2015, http://www.goa-on.org/resources/plans_strategies.php).

In this study, we combine two recently developed, low-powered technologies to observe near-full water column CO$_2$ and aragonite saturation state dynamics over the summer upwelling season in the coastal waters along the U.S. West Coast near La Push, Washington. Specifically, we deployed

and evaluated the performance of a prototype pCO$_2$ optical sensor, or optode, on a wave-powered "profiling crawler," or PRAWLER, in a novel application by parking the PRAWLER at specific depths on a mooring line to allow for equilibration of the optode sensor. Results from this study have the potential to not only help us better understand and monitor corrosive upwelling events, but also to be integrated into regional models to predict future corrosive events.

Materials and procedures

Study site

The Washington continental shelf, located in the northern part of the California Current System, contains the Olympic Coast National Marine Sanctuary (Fig. 1a). This region is a highly productive, nitrate-limited system, and even more productive than the Oregon and California shelves to the south (Hickey and Banas 2008; Alford et al. 2012). Compared to lengthy time series that exist in Oregon and California (Bograd et al. 2008; Chan et al. 2008; Nam et al. 2011), the Washington shelf is relatively understudied, in part due to extreme winter conditions that make sustained observations challenging. Steady northwesterly winds typically occurring from April to September cause warmer, fresher, low-nutrient surface waters to be transported offshore, driving local upwelling of colder, saltier, high-nutrient waters from depth. These nutrients help support large phytoplankton blooms, which then fuel the productive ecosystem. The cumulative effect of respiration in these originally deeper waters results in the upwelled high-nutrient waters also having lower O$_2$ concentrations, lower pH, and higher DIC concentrations. Upwelling, therefore, can contribute to enhanced OA and hypoxic events. The upwelled waters are then subject to additional respiration
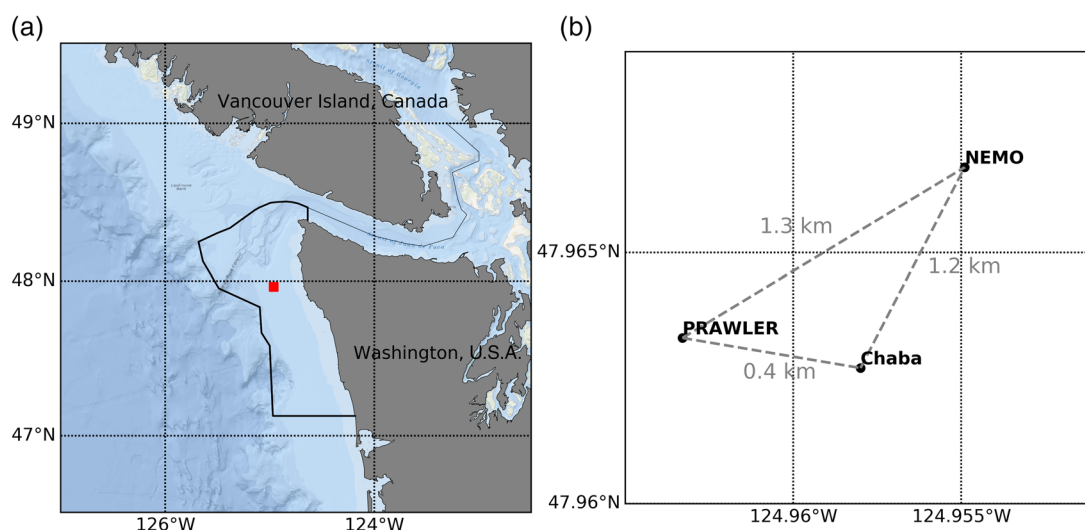

Fig. 1. (**a**) Location of study site (red square) off the coast of La Push, WA. Black line is the border of the Olympic Coast National Marine Sanctuary. (**b**) Inset of study site, which includes the Ćhá?ba· surface mooring, the Northwest Enhanced Moored Observatory (NEMO) subsurface profiler, and PRAWLER, which was deployed from 11 July 2017 to 23 September 2017 at 47.9633°N, 124.9633°W in 106 m of water.

on the shelf that subsequently reduces the O_2 concentrations to hypoxic levels during periods throughout the summer and early fall months (Connolly et al. 2010). Monitoring of acidified and hypoxic events has been especially important to the regional shellfish industry over the last decade after severe die-offs of larval oysters in Pacific Northwest hatcheries (Barton et al. 2012, 2015) and predicted declines in Dungeness crabs (Hodgson et al. 2018), which are economically significant fisheries to the region.

Moorings and sensors

The location was chosen for the optode test bed due to its proximity to the Northwest Enhanced Moored Observatory (NEMO), which is part of the Northwest Association of Networked Ocean Observing Systems (NANOOS, www.nanoos. org), and includes both surface and subsurface components (Alford et al. 2012, Fig. 1a). During this study, there were three fixed assets deployed at this location within 0.4–1.3 km of each other: the Ćháʔba· surface mooring, the NEMO subsurface profiler mooring, and the PRAWLER mooring (Fig. 1b). The Ćháʔba· surface mooring measures both atmospheric and oceanographic properties. Relevant to this study, within the upper meter of the surface, there is a conductivity-temperature-depth (CTD) package (SBE 16plusV2, Sea-Bird Scientific) measuring salinity, temperature, and O_2, as well as a Moored Autonomous pCO_2 system (MAPCO2™, Battelle Memorial Institute Seaology® pCO_2 monitoring system) and a Submersible Autonomous Moored Instrument for pH (SAMI-pH, Sunburst Sensors) (Seidel et al. 2008; Sutton et al. 2014, 2016). Approximately 1 km to the northeast on the NEMO subsurface mooring, there is a McLane Moored Profiler (McLane Research Laboratories), which moves up and down between 20 and 90 m depth along the mooring line and measures salinity, temperature, and O_2 as well as other oceanographic properties not relevant to this study.

NOAA Pacific Marine Environmental Laboratory (PMEL) developed the PRAWLER (Osse et al. 2015) and transferred the technology to McLane Research Laboratories, making it commercially available in 2019. For this study, the PRAWLER was deployed on 11 July 2017 and recovered on 16 October 2017. The PRAWLER is a small, 15 kg profiling instrument that uses surface wave action to ratchet up the mooring line from depth. It then free-falls at 30 cm s^{-1} to record a profile, making it capable of obtaining 20–30 profiles a day with 2–3 m vertical resolution. The PRAWLER includes real-time, two-way inductive and Iridium communication for control and data transmission to shore. It provides greater vertical sampling resolution than multiple sets of instrumentation fixed at specific depths along the mooring line and provides antifouling protection by staying out of the euphotic zone for the majority of the deployment. The tradeoff is that fixed-depth sensors can achieve higher temporal resolution at a specific depth. The PRAWLER also reduces the power load and cost of moored platforms. In addition to free-fall profiling mode, a fixed-depth

mode was developed for this deployment to allow for equilibration of the pCO_2 optode (Model 4797, Aanderaa Data Instruments). The PRAWLER also contained a modified CTD (Sea-Bird Scientific, repackaged SBE37), as well as a dissolved O_2 optode (Model 4330, Aanderaa Data Instruments). There was an additional instrument package positioned below the deepest PRAWLER depth at 88 m containing a CTD (SBE 16plusV2) with O_2 (Model 4831, Aanderaa Data Instruments) and pCO_2 optodes, as well as a SAMI-pH (Sunburst Sensors) (Fig. 2a,b). In addition to the fixed-depth assets, a Wave Glider equipped with an Autonomous Surface Vehicle CO$_2$ (ASVCO2™) system, effectively a repackaged MAPCO2™ (C. L. Sabine unpubl.), was driven near the location to provide additional validation measurements on 12 August 2017.

Detailed description of the sensing and operational principles of the pCO_2 optode can be found in Atamanchuk et al. (2014). Briefly, dissolved CO_2 diffuses from surrounding water through a gas-permeable membrane into the sensing layer of the optode, where pH is modified relative to the pCO_2 level outside the membrane. Change in fluorescent properties of the pH indicator inside the sensing layer is detected by the optode as a change in phase shift (φ) of sine wave-modulated light. The optode is capable of measuring a range of 0–50,000 μatm. Atamanchuk et al. (2014) reported response times (τ_{63}) varying from 45 s at 40°C to 4.5 min at 0°C in a stirred beaker. Reported precision was $\pm$ 2–3 μatm and absolute accuracy was 2–75 μatm (based on field data). Stability was shown to be longer than 7 months (Atamanchuk et al. 2014).

The pCO_2 optode was preconditioned by soaking for 2 weeks at a salinity of 34.2–34.4 and then calibrated at 21 points (seven pCO_2 concentrations and three temperatures) targeting the range of 250–1200 μatm at 5–25°C using a temperature-controlled water tank that was saturated with gas of varying CO_2 concentrations. Saturation values were checked against an independent G2201-i Analyzer CRDS CO_2 analyzer (Picarro). A 3D calibration model is calculated where log(pCO_2) is fit to a sixth by second degree polynomial that is dependent on φ and temperature. The initial calibration for the optode was later expanded to cover a broader range of pCO_2 values, because $pCO_2 > 1200$ μatm (the initial upper limit) was observed during the deployment. This procedure included fitting a second-degree polynomial to initial φ and pCO_2 data at each temperature ($R^2 = 0.9999$), adding calibration points for φ to increase the calculated pCO_2 range up to 2000 μatm, and updating calibration coefficients accordingly. The expansion of the initial calibration polynomial could be a source of error that will be described in a later section. After the optode is deployed, the sensing foil requires in situ conditioning with ambient seawater, which is a process that occurs on the order of days (Atamanchuk et al. 2014, 2015a,b).

Validation measurements

For surface validation, pCO_2 measured by the optode on the PRAWLER (henceforth referred to as PRAWLER optode pCO_2; Table 1) was compared to the measurements from the
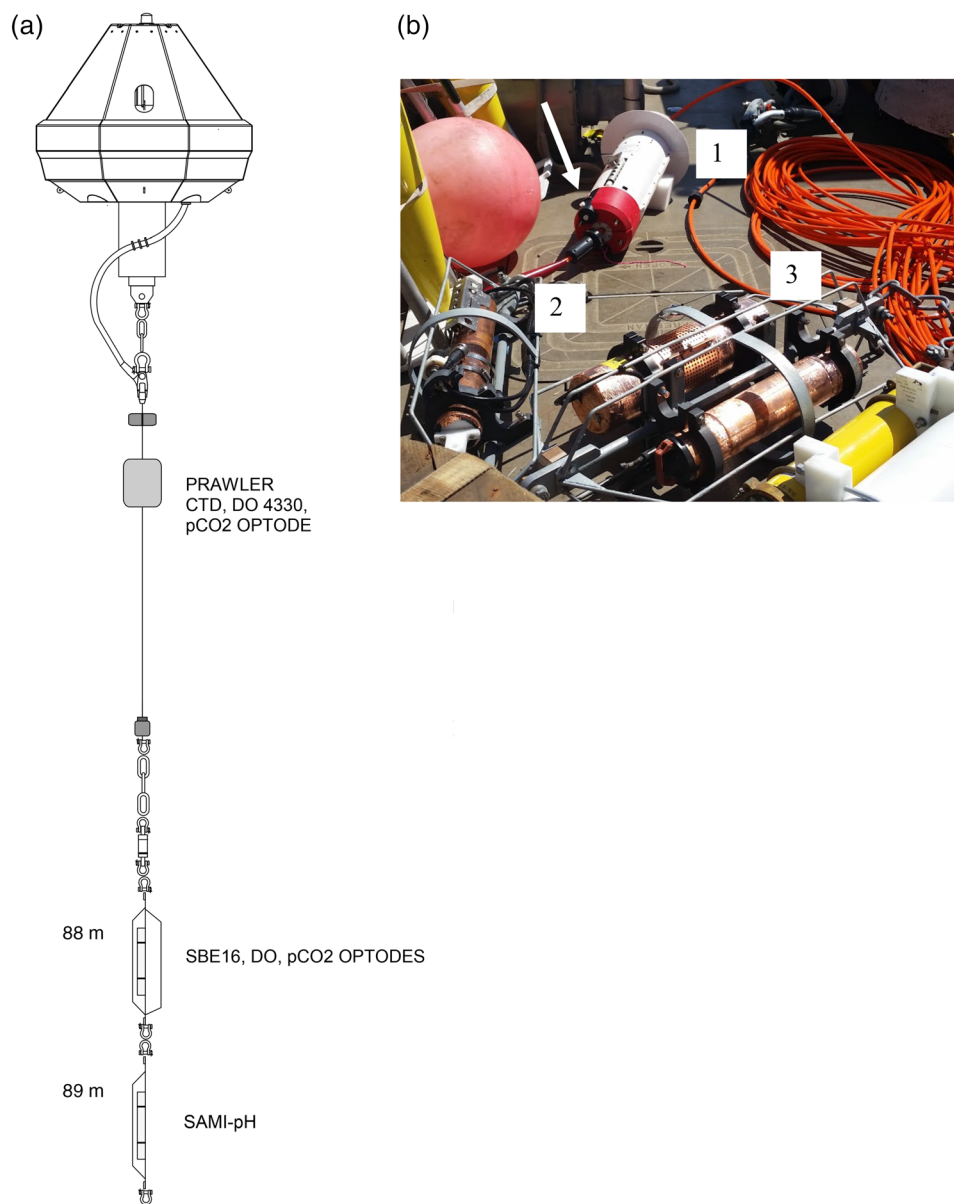
Fig. 2. (**a**) Schematic diagram of PRAWLER buoy and instrumentation located above the acoustic release. (**b**) Instruments deployed on the PRAWLER mooring: (1) PRAWLER with CTD, O$_2$ optode, and pCO$_2$ optode (white arrow points to optode position on PRAWLER, the casing was removed prior to deployment); (2) Seabird 16 CTD with O$_2$ and pCO$_2$ optodes; and (3) SAMI pH and external battery.

MAPCO2™ system on the Ćháʔba· mooring that sampled at ~ 0.5 m depth every 3 h (henceforth referred to as Ćháʔba· MAPCO2™; Table 1). The PRAWLER surface depth was between 3 and 6 m (due to range in swell height which caused the PRAWLER to heave up and down while clamped to the mooring line). In addition, PRAWLER optode pCO$_2$ measurements were compared to surface pCO$_2$ measured at ~ 0.5 m depth and within < 2 km by a Wave Glider ASVCO2™ system (henceforth referred to as ASVCO2™; Table 1).

For subsurface validation, we used empirical relationships developed for the northern California Current System, which are based on similar methodology to Alin et al. (2012), to estimate carbonate system parameters from 42°N to 50°N, 0 to 200 km offshore, and 0 to 100 m depth. A key assumption in the empirical algorithms is that the stoichiometry of the relationship between O$_2$ and DIC is primarily controlled by aerobic respiration in the water mass since it was last exposed to the atmosphere. Additionally, it is assumed that upwelling is the main process that brings these water masses to the continental shelf. Here the algorithm was extended to the surface; however, the different exchange rates of CO$_2$ and O$_2$ at the air–sea interface may result in a larger error in estimates generated in the upper 15–30 m of the water column by using the relationship between CO$_2$ and O$_2$. Surface heating or cooling

Table 1. Data sets assessed for pCO_2 optode performance and their description. See Fig. 1 for platform locations.

Data set name	Data set description
PRAWLER optode pCO_2	pCO_2 measured by the Aanderaa pCO_2 optode on the PRAWLER (either raw measurements or adjusted using algorithm reference data)
Ćháʔba· MAPCO2™	pCO_2 measured by the MAPCO2™ system on the Ćháʔba· surface buoy
ASVCO2™	pCO_2 measured by the ASVCO2™ system on the surface wave glider
Modeled PRAWLER pCO_2	pCO_2 calculated by algorithm-derived DIC (Eq. 1) and TA (Eq. 2) using T, S, and O_2 measurements from the PRAWLER

will also change how temperature affects the relationships. The empirical algorithms (Eqs. 1, 2) use oxygen (O_2 in μmol kg^{-1}), temperature (T in °C), salinity (S), and the potential density anomaly (σ_θ in kg m^{-3}) to calculate DIC and TA.

$$\left[\text{DIC } \mu\text{mol kg}^{-1}\right] = 955.6636926 - 0.776753102 {}^{*}O_2 \quad (1)$$
$$+ 51.19911384 {}^{*}\sigma_\theta$$

$$\left[\text{TA } \mu\text{mol kg}^{-1}\right] = 673.4949547 + 44.53461935 {}^{*}S \quad (2)$$
$$+ 4.049611464 {}^{*}T + 278.5666762 {}^{*}1/T$$

These relationships achieved R^2 values of 0.97 and 0.90 and root-mean-squared errors (RMSEs) of 18 μmol kg^{-1} and 12 μmol kg^{-1} for DIC and TA, respectively, for the calibration data set of National Oceanic and Atmospheric Administration Ocean Acidification Program West Coast Ocean Acidification (NOAA OAP WCOA) cruises from 2007 to 2016 (Feely and Sabine 2013; Feely et al. 2015, 2016b,c; Alin et al. 2017). Estimated DIC and TA were then used to calculate pCO_2 concentrations using CO2SYS (Lewis and Wallace 1998; van Heuven et al. 2011; Orr et al. 2018) using carbonate (Lueker et al. 2000), sulfate, and borate equilibrium constants (Dickson 1990a,b). Phosphate and silicate equilibrium constants are from Millero (1995) and total boron is calculated using Uppstrom (1974). pCO_2 calculated from the algorithms using PRAWLER hydrographic data will be referred to as modeled PRAWLER pCO_2 (Table 1). Modeled PRAWLER pCO_2 had an average estimated uncertainty of ~ 16% based on propagating the RMSE for TA and DIC in the CO2SYS calculation of pCO_2 (Orr et al. 2018). The average error of the modeled PRAWLER pCO_2 relative to high-quality Ćháʔba· MAPCO2™ (< 2 μatm uncertainty) was found to be 13%, which is within the model uncertainty. Note that only data from the most equilibrated PRAWLER periods when the PRAWLER and Ćháʔba· buoys were measuring the same source waters (defined here as $\Delta T < 0.5$ and $\Delta S < 0.5$) was used.

Discrete bottle samples were taken the day after the mooring was deployed. However, the pCO_2 optode was not fully conditioned such that the bottle samples could not be used as a reference for the optode measurements. Prior to recovery of the instrument package, the PRAWLER ran out of power before it was possible to take validation bottle samples. Therefore, DIC and TA from collected bottle samples were used to compare to algorithm-calculated DIC and TA using measured parameters during sample collection. The resulting RMSE between the modeled and bottle data for DIC was larger than the model suggests at 26 μmol kg^{-1} instead of 18 μmol kg^{-1}, but lower than the model TA RMSE at 5 μmol kg^{-1} instead of 12 μmol kg^{-1} ($n = 16$ for DIC and TA, from sampled depths 2–87 m). Although we intended to also compare the pCO_2 and pH measured by the instrument package at the bottom of the mooring line, there were multiple instrument failures due to a faulty voltage channel on the CTD, and the data were unrecoverable.

Assessment

PRAWLER vehicle performance

The carbon PRAWLER package was deployed on 11 July 2017 and recovered on 16 October 2017. The battery on the PRAWLER lasted until 23 September after conducting 614 profiles over 74 d. The PRAWLER obtained 7–8 profiles per day with 0.5–1 h between profiles and each profile took 2–3 h to complete. As mentioned previously, the PRAWLER was used primarily in fixed-depth mode during this deployment. There were nine depth stations set at approximately 10 m intervals (4, 10, 20, 30, 40, 50, 60, 70, and 80 m), although actual depth of sampling could vary by 1–4 m depending on swell height. At each depth station, the PRAWLER would first be parked at the specified depth and not record data, a so-called soak period, and then sample continuously at an 8 s interval for 8 min. After finishing the sampling period, the PRAWLER would move down to the next depth. After reaching the bottom, the PRAWLER would ratchet up and down the mooring line until it was time to begin the next profiling cycle starting at the surface. With two-way iridium communication, we had the ability to receive data from the PRAWLER and change any of the sampling settings in real time from shore.

Observed patterns in PRAWLER T, S, and O_2 measurements

Data from the first 2 weeks of the deployment were not considered in the data analysis due to optode in situ conditioning, which is typically on the order of days (Atamanchuk et al. 2014, 2015a,b). Over the remaining deployment period, temperature ranged between 7°C and 17°C with temperatures > 10°C found in the top 20 m (Fig. 3a,b). Salinity in near-surface (3–6 m) waters was as low as 30.5 in the beginning of the deployment and increased to ~ 32 by the end of July, and stayed within 32 ± 0.5 until the end of the deployment (Fig. 3c,d). Salinity increased with depth and was ~ 34 at the 80 m depth station throughout the deployment. There was strong stratification due
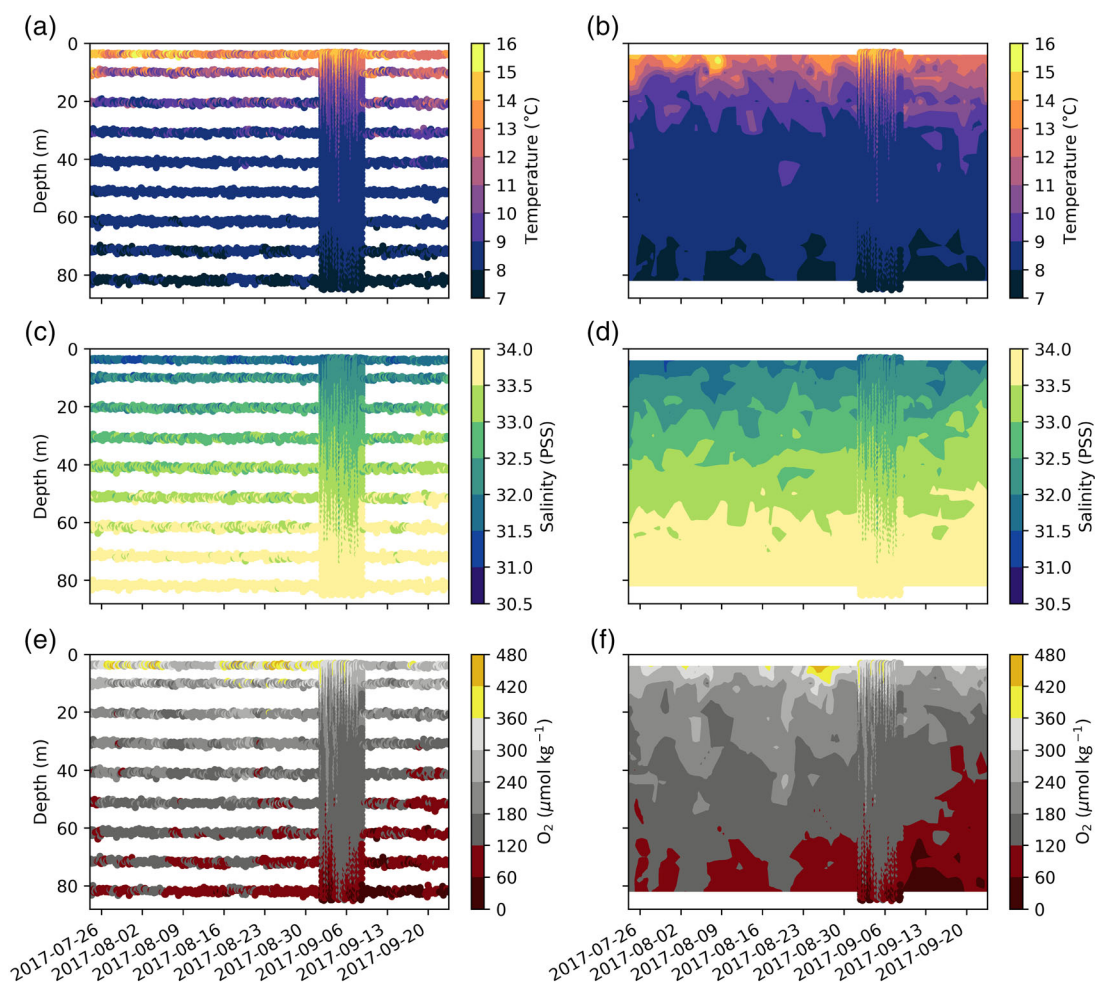
Fig. 3. Temperature (**a**, **b**), salinity (**c**, **d**), and dissolved O$_2$ (**e**, **f**) measured on the PRAWLER throughout the deployment. Panels on the left are PRAWLER data directly measured at fixed depths except during the free-fall profiling period in early September 2017. Panels on the right are contour plots with filled intervals and the free-fall profiling data are overlaid.

to the warmer, fresher waters on the surface and colder, saltier waters at the deeper depths.

In addition to temperature and salinity effects on oxygen solubility and mixing with upwelling waters, O$_2$ concentrations were also influenced by biological processes such as production and respiration. Dissolved O$_2$ concentrations ranged approximately from 300 to 500 μmol kg-sw^{-1} in near-surface (3–6 m) waters (Fig. 3e,f). This translates to 80–200% O$_2$ saturation, where O$_2$ was supersaturated (> 100%) for 75% of the deployment. At ~ 80 m, O$_2$ concentrations were between 80 and 120 μmol kg-sw^{-1} until 10 September, and afterward, values decreased to 5–100 μmol kg-sw^{-1} translating to 1–35% saturation. These O$_2$-depleted waters (< 120 μmol kg-sw^{-1}) reached depths as shallow as 40 m toward the end of the deployment, where hypoxic waters (< 60 μmol kg-sw^{-1}, shown in dark red Fig. 3e,f) are present through the rest of the deployment. Cold, low-oxygen water intrusions are apparent in approximately week-long periods in the deeper water column throughout the deployment. Periods of hypoxic waters

were also seen at 85 m in September 2014 and 2016 at the nearby Ćháʔba· mooring (PSEMP Marine Waters Workgroup 2017). These low O$_2$ waters were often associated with southerly winds and currents and advected northward along the shelf based on data collected on the ASVCO2™ as well as the NEMO and Olympic Coast National Marine Sanctuary buoys (PSEMP Marine Waters Workgroup 2017). These observations were seen previously in this region by Connolly et al. (2010) in 2005 and by the Puget Sound Marine Waters Workgroup in last several years.

Optimal equilibration time for *p*CO$_2$ optode

Response time of the *p*CO$_2$ optode is mainly affected by temperature, salinity, and flow rate over the sensing foil. Temperature is a primary factor affecting response time of the optode: diffusion of CO$_2$ into the sensor foil is slower in colder water. The response time (τ_{63}) reported in Atamanchuk et al. (2014) was 4 min at 0.5°C, meaning that 99% equilibration would take ~ 18 min, while response time at 20°C was
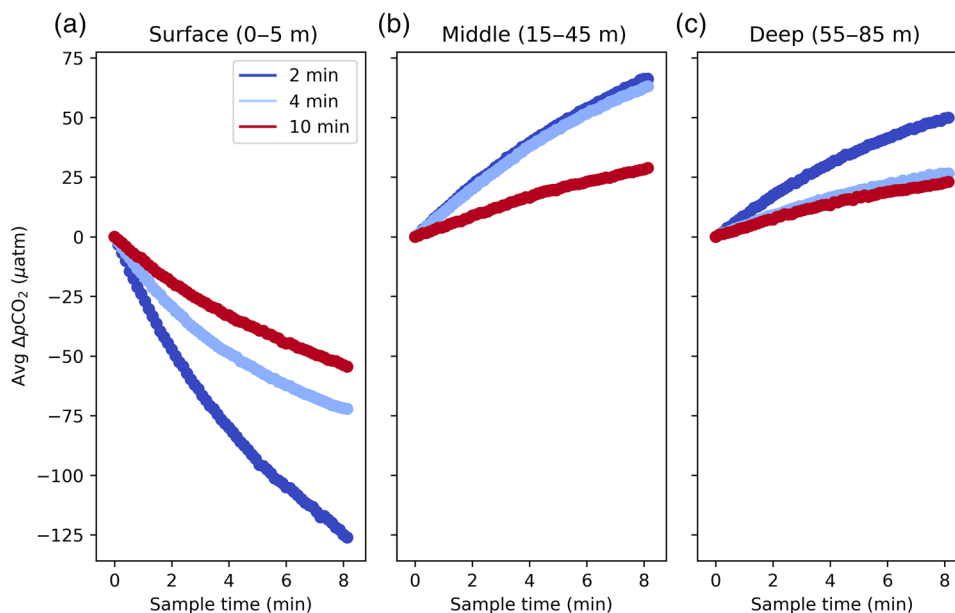
Fig. 4. Equilibration curves for different soak periods for the optode are shown for (**a**) surface (0–5 m), (**b**) middle (13–45 m), and (**c**) deep (55–85 m). Each line plotted represents the average time it took to get from the first measurement point to the last (most equilibrated) for a depth bin. The y-axis is the pCO_2 difference from each average pCO_2 measurement point relative to the first average pCO_2 for that soak period.

45 s. The temperature is measured with a built-in sensor on the optode as well as with the CTD on the PRAWLER. The optode may also drift out of calibration temporarily after extended exposure to salinity that is > 1 salinity unit different from the salinity used for optode calibration due to the so-called "osmotic effect," which is a result of the osmotic pressure between different salinities. This issue was avoided by parking the optode at depth and close to its calibration salinity of 34.2–34.4 when not profiling. While each profile took 2–3 h, there was not a sustained period of time in a significantly different salinity and, therefore, it did not affect the optode calibration. Pressure effects are negligible at < 100 m. Storage and conditioning affect accuracy of optode measurements, but do not influence response time, that is, speed of equilibration.

The first objective for the deployment was to find the optimal amount of time needed to reach full equilibration for the pCO_2 optode. In this study, we tested soak times of 0, 2, 4, and 10 min followed by sampling at an 8 s interval for 8 min. Data presented herein (exclusive of Fig. 4) are the mean of the last minute of sampling at each parked depth, which contained the last seven measurements. This method used the most equilibrated data available. Total time was calculated as soak time in addition to sampling time, where the longest equilibrated measurement at a specific depth was 18 min. From 02 to 09 September, there was no soak time, or in other words, the PRAWLER was in free-fall/profiling mode (see full profile data in Fig. 3a,c,e), which did not provide usable data for the pCO_2 optode (this will be discussed further in the next section). Free-fall profiling mode does, however, provide reliable *T*, *S*, and O_2 data (Fig. 3a,c,e).

The pCO_2 optode data were categorized by periods of soak time (2, 4, or 10 min) to find the appropriate length of time needed at a fixed depth to achieve full equilibration. For each soak time in surface (0–5 m), middle (15–45 m), and deep (55-85 m) depths, pCO_2 was averaged over the 8-min sampling period and the average pCO_2 difference (ΔpCO_2) was found by subtracting the first average pCO_2 from the average pCO_2 at each 8-s sampling interval (Fig. 4). Negative ΔpCO_2 values are seen in the surface due to the large vertical pCO_2 gradient where the optode was exposed to higher pCO_2 in the colder, deeper waters before equilibrating to much lower pCO_2 in the warmer surface waters (Fig. 4a). Throughout the water column, the 10-min soak time data had the smallest range in average ΔpCO_2 and therefore, shallowest slopes, while the 2-min soak time data had the largest average ΔpCO_2 and steeper slopes (Fig. 4). This is because the disequilibrium for pCO_2 is higher after the 2-min soak time than after the 10-min soak time. For example, for the deep bin, where average temperature was ~ 8°C, fitting an exponential to each equilibration curve led to 72%, 76%, and 89% equilibration after 2-min, 4-min, and 10-min soak times, respectively. It would have taken 37–40 min for 99% equilibration, which is almost double the time of ~ 21 min for 99% equilibration in a stirred beaker at 0.5°C (Atamanchuk et al. 2014), and 55–59 min for 99.9% equilibration.

Faster equilibration would be expected for warmer temperatures in surface waters; however, during this deployment, there was faster equilibration at deeper, colder depths (Fig. 3a, b). This could be because the optode equilibration time is affected by a combination of temperature and pCO_2 concentration gradients. Both absolute temperature values as well as

temperature gradients are important to consider in their effects on optode response time for this deployment. At depths shallower than 20 m, there is a larger temperature gradient, while at depths greater than 20 m, temperature was approximately the same. In between measurement profiles, the PRAWLER was moving up and down the mooring line to maintain the optode calibration by not sitting outside its calibration salinity for a sustained period. This may have led to insufficient time, especially at shorter soak times, for the optode to equilibrate at the surface due to the significant temperature change between the surface and subsurface depths. Due to the lack of sufficient active flow over the membrane and the membrane proximity to the titanium sensor body, the $p\mathrm{CO_2}$ optode may have developed a memory effect of colder, higher $p\mathrm{CO_2}$ bottom waters.

Each soak period reached at least 63% equilibration at middle and deep depths; however, if we define "fully" equilibrated as within 2 μatm for the last minute, the only fully equilibrated data at middle depths is the 10-min soak time and at deeper depths, the 4- and 10-min soaks. Hence, a 10-min soak time, or 18-min equilibration gave the most equilibrated data, although not necessarily 100% equilibrated data, at all depths. Equilibration times reported by Atamanchuk et al. (2014) were similar for colder temperatures (~ 21 min at 0.5°C) measured in a well-stirred beaker. The optode should have been able to achieve shorter (< 21 min) equilibration times during this deployment where lowest temperatures reached 7°C, but required longer equilibration times due to the absence of sufficient active flow. Faster equilibration times for optodes can be achieved by using pumped seawater to increase the flow against the sensor foil which decreases the boundary layer for improved diffusion (Bittig et al. 2018).

Optode adjustment using algorithm reference data

Following procedures described by Atamanchuk et al. (2014), we used modeled PRAWLER $p\mathrm{CO_2}$ from 80 m as reference data to calculate an offset adjustment to the calibration model that uses $\log(p\mathrm{CO_2})$ as a function of phase shift and temperature. This adjustment corrects for any conditioning, storage-related, or instrument drift. At 80 m, the algorithm model is not degraded by surface ocean biological productivity and air–sea gas exchange. Hence, raw optode (phase shift φ) measurements were taken from the uncorrected PRAWLER optode $p\mathrm{CO_2}$ at 80 m, and an adjustment was made to minimize the average residual between PRAWLER optode $p\mathrm{CO_2}$ and modeled PRAWLER $p\mathrm{CO_2}$ at the same depth and time (Fig. 5d,e). Only sections of the most equilibrated (10-min soak) data were used for this adjustment. A correction was applied to each of the three sections of 10-min soak data excluding the low $\mathrm{O_2}$/high $\mathrm{CO_2}$ period after 13 September (Period 1: 03–17 August, Period 2: 28 August–02 September, and Period 3: 08–13 September, *see* Figs. 5, 6), and a linear drift over time was assumed for the adjustments for data between 10-min sections. Data were interpolated to hourly

increments for comparison purposes. Before adjustment, the mean residual between the uncorrected PRAWLER optode $p\mathrm{CO_2}$ and modeled PRAWLER $p\mathrm{CO_2}$ was -265 ± 83 μatm or -18%, suggesting a fairly large offset and scatter as well as an overall drift of ~ 5.5 μatm a day from the first day of deployment (Fig. 5d). After adjustment for each 10-min soak period was corrected for the drift and offset, the mean residual was -1 ± 35 μatm or -0.2% with $n = 508$ and $R^2 = 0.96$ for all points in the 10-min sections not including after 13 September (Fig. 5e, Table 2). For all of the data at 80 m including the 2- and 4-min soak periods, the mean residual was -5 ± 39 μatm or -0.6% with $n = 1454$ and $R^2 = 0.98$, suggesting that the assumption of a linear drift between 10-min sections was valid. These adjustments were then expanded to all depths to provide the adjusted PRAWLER optode $p\mathrm{CO_2}$ that will be reported from here on.

Although Ćhá?ba· $p\mathrm{CO_2}$ surface data could have also been used as reference data to adjust the PRAWLER optode $p\mathrm{CO_2}$, we did not choose this method due to multiple factors: (1) If Ćhá?ba· $p\mathrm{CO_2}$ were used as reference data, the mean residual between Ćhá?ba· $p\mathrm{CO_2}$ and PRAWLER optode $p\mathrm{CO_2}$ (adjusted to Ćhá?ba·) would be -2 ± 32 μatm ($n = 200$) (not shown), which is similar to -1 ± 35 μatm ($n = 508$) using the 80 m algorithm but the algorithm provides a larger number of comparison data points (Fig. 5); (2) The algorithm performs adequately in the surface where modeled Ćhá?ba· $p\mathrm{CO_2}$ (the algorithm is calculated with input parameters from the Ćhá?ba· mooring) compared to measured Ćhá?ba· $p\mathrm{CO_2}$ resulted in average offset of 22 ± 18 μatm or an 8% error (Fig. 5c), which is within the stated uncertainty of the model at 16%. This offset and scatter is likely due to biological activity and different air–sea gas exchange rates in the surface ocean impacting reliability of the algorithm. In addition, both the model and Ćhá?ba· suggested similar drift in the uncorrected or raw optode measurements at 80 m and the surface, respectively ($y = -3.5x + 104.9$ and $y = -5.6x - 44.5$, where x is the number of days since deployment) (Fig. 5a,d); (3) There is a drift of ~ 2 μatm d^{-1} between the Ćhá?ba· and adjusted PRAWLER $p\mathrm{CO_2}$ suggesting that there is still environmental variability between the Ćhá?ba· and PRAWLER moorings that is not accounted for by considering when locations have similar temperature and salinity. Using the 80 m algorithm-based estimates as a reference eliminates spatial differences and environmental variability between the Ćhá?ba· and PRAWLER mooring locations (0.4 km away from each other) and differences in sampling depths (0.5 m for Ćhá?ba· and 3–6 m for PRAWLER).

Optode $p\mathrm{CO_2}$ observations and comparison to other observations/models

After allowing for 2 weeks of conditioning for the optode from 11 July to 24 July (data not shown), adjusted PRAWLER optode $p\mathrm{CO_2}$ ranged approximately from 70 to 760 μatm in near-surface waters (Figs. 6c, 7a). Values under 200 μatm fall
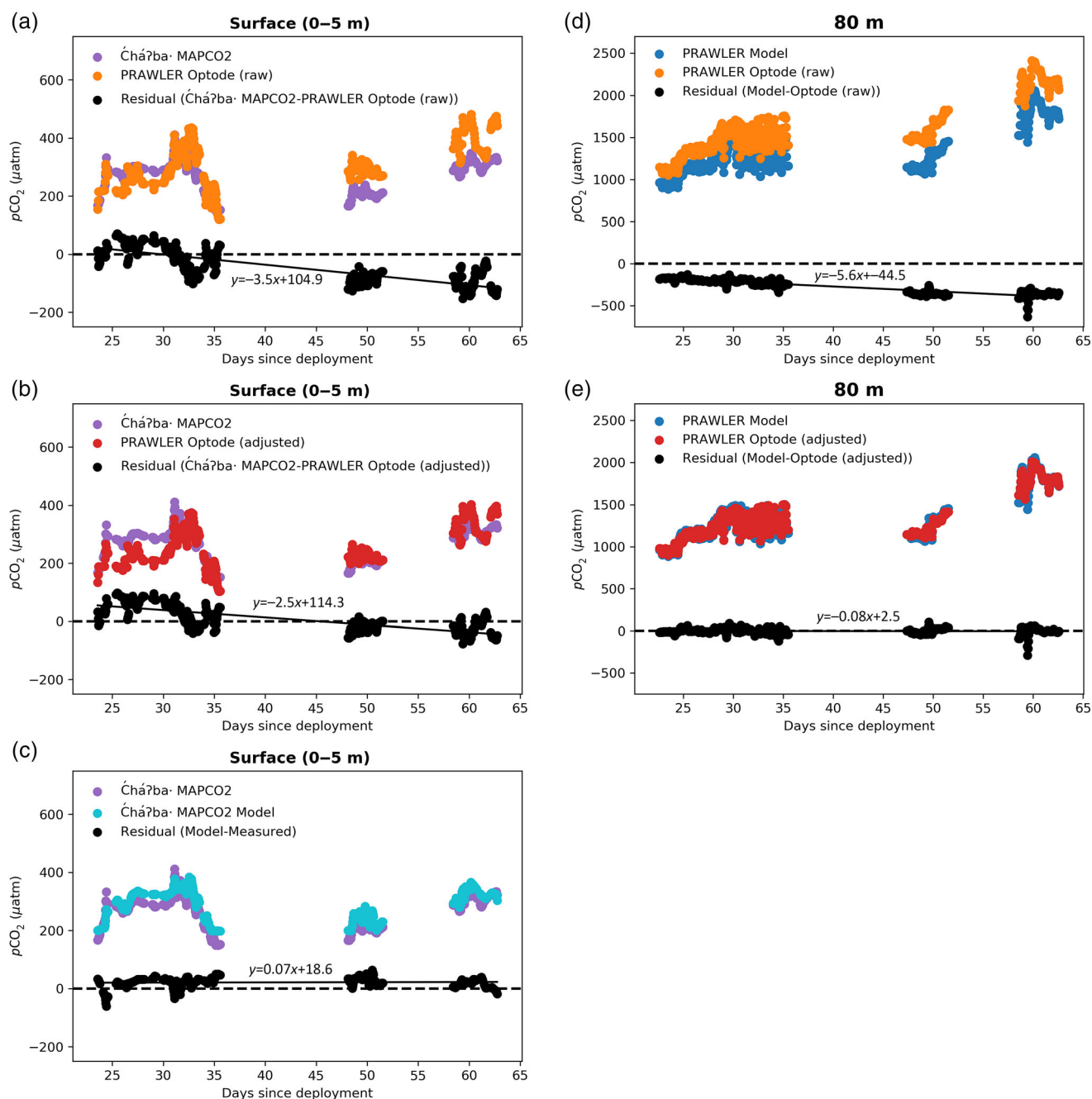
Fig. 5. pCO_2 measured during the three sections of 10-min soak data excluding the low O_2/high CO_2 period after 13 September (Period 1: 03–17 August, Period 2: 28 August–02 September, and Period 3: 08–13 September). Ćháʔba· MAPCO2™ data are either measured and modeled using algorithms and only from periods when the two locations are measuring similar water masses ($\Delta T < 0.5$ and $\Delta S < 0.5$). PRAWLER optode data are shown as raw measurements, modeled using algorithms, and adjusted per period using 80 m reference algorithm data. Surface comparisons are shown in (**a**–**c**) and 80 m comparisons are shown in (**d**, **e**). Residuals (black) are shown with a line of best fit. The x-axis is the number of days since the deployment (11 July 2017) to show how the measurements drift after the deployment.

below the calibration lower limit of the optode and therefore may be less accurate. At 80 m, concentrations ranged from 1000 to 2000 μatm. The highest pCO_2 values at 80 m occurred in the second to last week of the deployment with sustained values > 1500 μatm. This occurs simultaneously with the

arrival of low O_2 waters (Fig. 3) due to the advection of hypoxic waters from the south.

The pCO_2 observations from the Ćháʔba· MAPCO2™ and ASVCO2™ have the lowest uncertainty of the validation data sets (Sutton et al. 2014), and therefore, were the primary

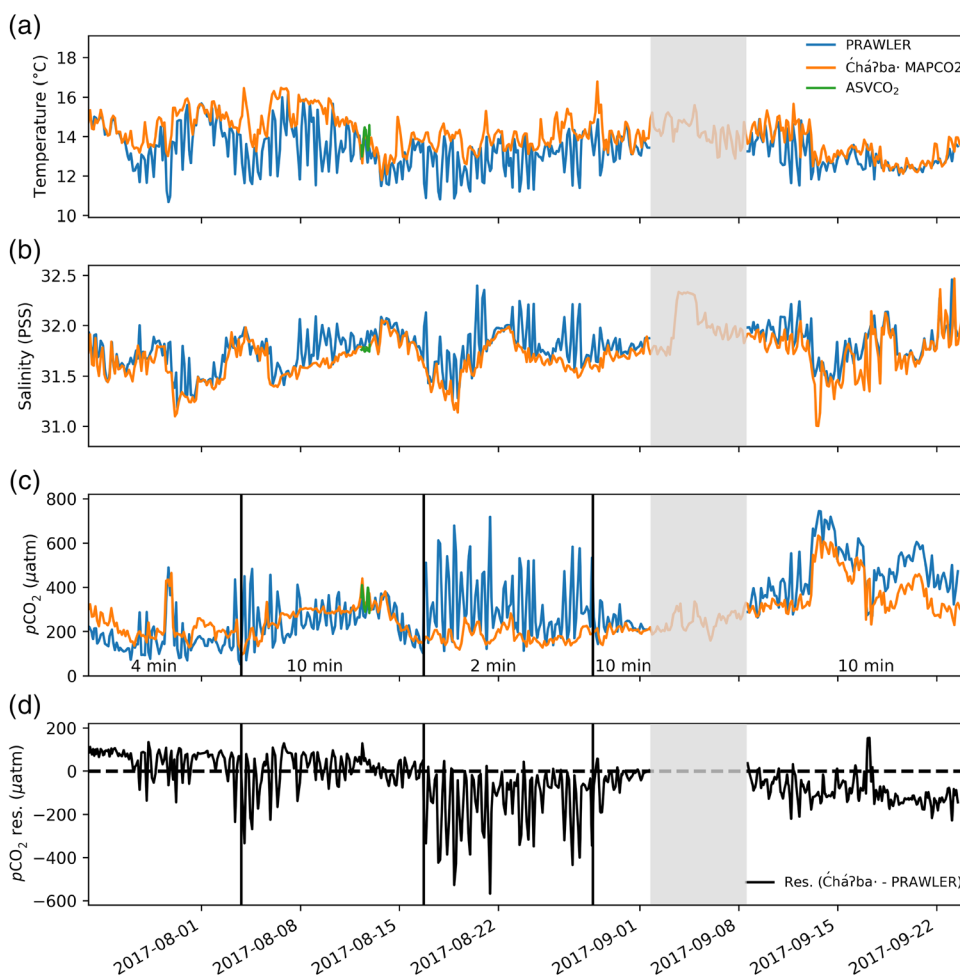**Fig. 6.** Surface data plotted from the PRAWLER and Ćháʔba· moorings as well as the Wave Glider ASVCO2™ (**a**) SST, (**b**) SSS, (**c**) surface seawater pCO$_2$, and (**d**) pCO$_2$ residuals between the PRAWLER (adjusted to 80 m algorithm data) and Ćháʔba·. The shaded region indicates the PRAWLER free-falling profile period, for which the pCO$_2$ data are not shown due to insufficient equilibration. The 2, 4, and 10 min labels in (**c**) refer to the soak times for each period of time.

focus for estimating the total error in the adjusted PRAWLER optode pCO$_2$ data. However, significant variability in the PRAWLER data hinders comparison among data sets. Surface seawater temperature (SST), salinity, and pCO$_2$ data collected from the PRAWLER are much noisier than Ćháʔba· data (Fig. 6). One likely factor is the differences in the sampling locations, including differences in surface depth of measurements (3–6 m for the PRAWLER and 0.5–1 m for Ćháʔba·) and the distances between the two moorings (0.4 km; Fig. 1b). The high near-surface stratification and heave of the PRAWLER, in combination with the slow equilibration time of the optode, all play a role in the larger variability of the PRAWLER data. The impact of equilibration time on the pCO$_2$ optode is also apparent during the section of the deployment with a 2-min soak time. The shorter equilibration time clearly causes increased variability in pCO$_2$ from the optode (Fig. 6c,d).

Despite the noise in the data, similar patterns are seen in both data sets. Sea surface temperature at Ćháʔba· is at the high end of the PRAWLER SST, which corresponds to Ćháʔba· measuring shallower, warmer surface water. Sea surface salinity (SSS) is the opposite, where Ćháʔba· SSS is at the low end of the PRAWLER SSS, likely because the Ćháʔba· CTD was measuring shallower surface water that was also less saline. During the period from 13 to 18 September, the PRAWLER optode pCO$_2$ increases approximately from 400 μatm from the week before to a peak of ~ 800 μatm, which is a similar magnitude of increase as the Ćháʔba· MAPCO2™ data ~ 300 μatm to a peak of ~ 600 μatm, or approximately a doubling of absolute surface seawater pCO$_2$ values. During this period, surface PRAWLER optode pCO$_2$ measurements are routinely higher than Ćháʔba·, which could be partially a result of measuring

Table 2. Average residual pCO_2 between the pCO_2 optode and validation data sets (pCO_2 from validation data set – pCO_2 from PRAWLER optode adjusted to the 80 m modeled reference data) with 1σ standard deviation (SD). Surface validation data sets from Ćháʔba· MAPCO2™ only include data when both locations are sampling the same water mass ($\Delta T < 0.5$ and $\Delta S < 0.5$) and when the ASVCO2™ was within 2 km, and subsurface comparison data set (modeled PRAWLER pCO_2) only include data for the 10-min soak periods excluding the low O_2 advection period after 13 September.

Depth	Distance to PRAWLER mooring (km)	Validation data set	Average residual $\pm$ SD compared to PRAWLER optode pCO_2 (μatm)	% Difference	RMSE (μatm)	n
Surface (0.5 m)	0.4	Ćháʔba· MAPCO2™	6 ± 42	2	43	200
Surface (0.5 m)	<2	ASVCO2™	35 ± 31	16	46	10
Water column (3–80 m)	0	Modeled PRAWLER pCO_2	-28 ± 66	−6	72	1337
Bottom (80 m)	0	Modeled PRAWLER pCO_2	-1 ± 35	−0.2	35	508

slightly deeper, cooler, and more saline water; however, the optode is measuring the same proportion of change. This large pCO_2 increase could be a result of the upwelling of CO_2-rich, hypoxic waters advected from the south.

In order to estimate PRAWLER optode pCO_2 error and uncertainty, we control for both environmental variability between the PRAWLER and Ćháʔba· buoys as well as the period of short equilibration time. First, as a control to equilibration time, we only consider Ćháʔba· and PRAWLER data when the SST and SSS suggest both locations are sampling the same water mass (ΔSST < 0.5 and ΔSSS < 0.5). In addition, we only consider data from 10-min soak periods and exclude the high CO_2 and low O_2 period after 13 September. Data are interpolated to hourly intervals to enable better comparison among the three measurements of the PRAWLER, Ćháʔba·, and ASVCO2™. The average residual between Ćháʔba· MAPCO2™ and adjusted PRAWLER optode pCO_2 (or pCO_2 from Ćháʔba· – pCO_2 from PRAWLER optode adjusted to the 80 m modeled reference data) is 6 ± 42 μatm or 2% error ($n = 200$; Table 2). ASVCO2™ pCO_2 data taken from within < 2 km of the PRAWLER mooring have an average residual of 35 ± 31 μatm or 16% error ($n = 10$) compared to PRAWLER optode pCO_2.

Although the modeled pCO_2 uncertainty is much larger than the primary validation data sets from the MAPCO2™ and ASVCO2™, the full profile data from the model provide another independent approach for evaluating the PRAWLER optode pCO_2. Modeled PRAWLER pCO_2 (Fig. 7c,d) follows similar patterns as the PRAWLER optode pCO_2 (Fig. 6a,b) and ranged approximately from 130 to 560 μatm in the surface waters to ~ 2000 μatm at depth. Values above the threshold for hypercapnia ($pCO_2 > 1000$ μatm, outlined in black Fig. 7b,d; McNeil and Sasse 2016; Feely et al. 2018) are present in the bottom water through most of the deployment. The highest concentrations of

$pCO_2 > 1500$ μatm are seen at depth toward the end of the deployment and co-occur with a low O_2 (Fig. 3) and high surface pCO_2 signal (Fig. 6). Taking a closer look at residuals between the optode and model pCO_2 (Fig. 7e,f), there are a few key areas where the optode and model differ significantly. Apart from the free-falling profiling period and the last 2 weeks of the deployment, the PRAWLER optode pCO_2 shows values lower than modeled PRAWLER pCO_2 in the top 20 m with positive residuals. The differences in exchange rates of O_2 and CO_2 at the air–sea interface that would alter the linear relationship between O_2 and CO_2 assumed in the empirical algorithm model (Alin et al. 2012) can explain the observed differences between the model and optode pCO_2. Since the optode is adjusted using data at 80 m, the relationship between O_2 and CO_2 in deep water that is largely influenced by respiration may not be as accurate for near-surface waters where processes such as photosynthesis and air–sea gas exchange drive concentrations of O_2 and CO_2.

Overall, depths below 20 m show a neutral to slightly negative residual, indicating the optode pCO_2 measurements tend to be higher than modeled pCO_2. This is particularly apparent in the last 2 weeks of the deployment (during the period of time that experienced advection of hypoxic waters from the south), which shows stronger negative residuals through most of the water column. This result is not surprising given that low-oxygen water masses advected from the south tend to have undergone significant in situ respiration on the shelf after their initial upwelling onto the shelf (Connolly et al. 2010; Siedlecki et al. 2015, 2016). Thus, the fundamental relationships underpinning the algorithm have been altered under these conditions.

For the 10-min soak periods (excluding the last 2 weeks of Period 3 that contained the low O_2 waters), the average residual between PRAWLER optode pCO_2 and modeled PRAWLER pCO_2 was -28 ± 66 μatm ($n = 1337$), or −1%, and RMSE of 72 μatm. This RMSE is larger than errors between the pCO_2
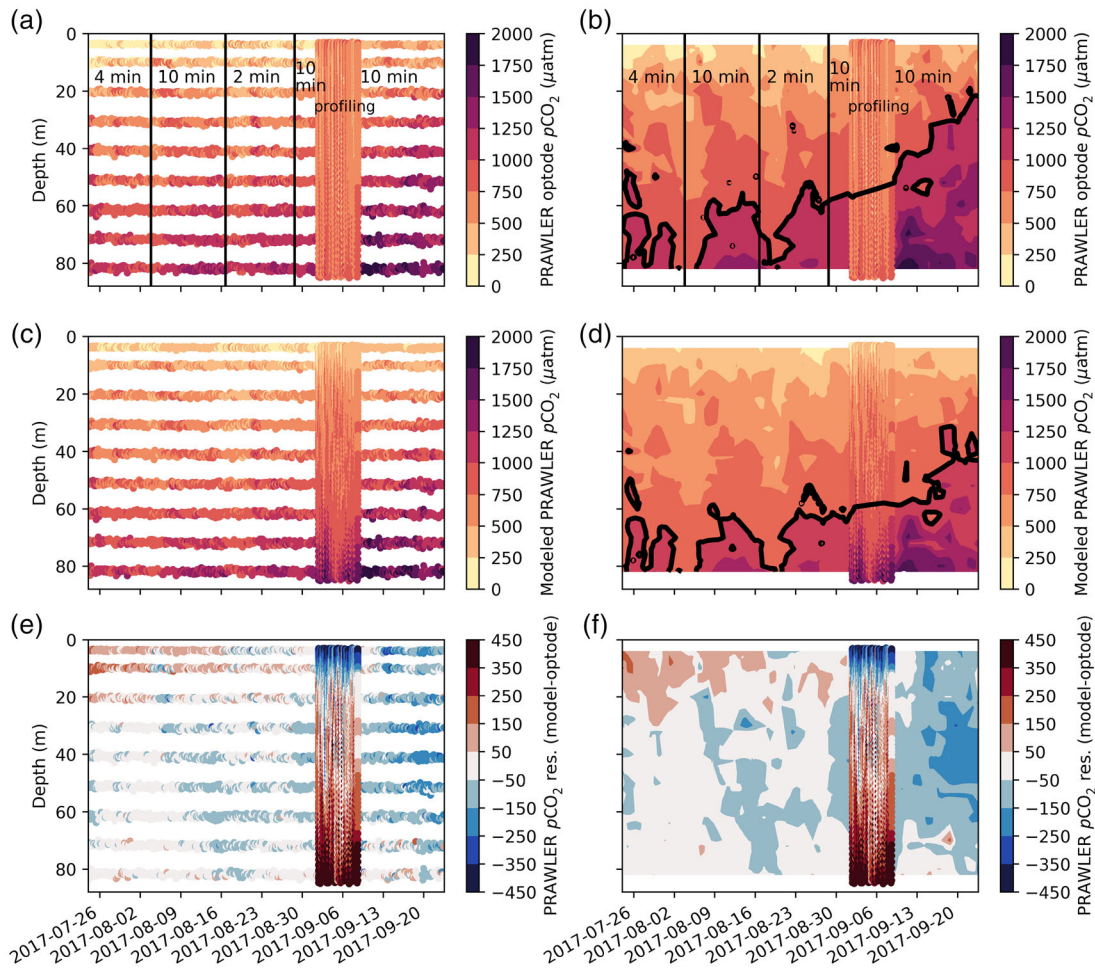
Fig. 7. Seawater pCO_2 from different sources: (**a, b**) PRAWLER optode (adjusted), (**c, d**) modeled PRAWLER, and (**e, f**) residuals between the PRAWLER optode and modeled PRAWLER. Panels on the left are PRAWLER data directly measured at fixed depths except during the free-fall profiling period in early September. Panels on the right are contour plots with filled intervals and free-fall profiling data overlaid. The black line highlights the 1000 μatm threshold for hypercapnia using contoured data only.

optode and MAPCO2™ and ASVCO2™ observed at the surface (Table 2), which is likely due to additional algorithm errors. Additionally, this larger error could be affected by the expansion of the optode calibration polynomial to accommodate pCO_2 values > 1200 μatm, values that are seen primarily at depths > 60 m. Therefore, the uncertainty of 72 μatm based on the RMSE is likely an upper bound estimate because it includes adjustment and algorithm errors as well as environmental factors.

Applying PRAWLER measurements to calculate aragonite saturation state

Aragonite is a calcium carbonate mineral that many organisms use to form their shells. We can use aragonite saturation state (Ω_{ar}) as an indicator of ecosystem health and vulnerability to OA, particularly for shell-forming organisms (Bednaršek et al. 2017). The ability to measure aragonite saturation state variability in the Northern California Current, both spatially and temporally, is of

great interest to local fisheries of oysters, Dungeness crabs, et al that have strong sensitivities to Ω_{ar}, especially when Ω_{ar} reaches below species-specific biological thresholds. Here we compare calculations of Ω_{ar} using two methodologies in order to determine feasibility of different sensor packages for observing OA on a PRAWLER. First, Ω_{ar} is calculated using an empirical algorithm similar to those for DIC (Eq. 1) and TA (Eq. 2) based on methodology by Alin et al. (2012), using temperature and dissolved O_2 concentrations (Eq. 3, Fig. 7a):

$$\Omega_{ar} = -17.167825 + 1.52647616*T + 0.00547706*O_2 \\ + 60.5017384*1/T - 0.038633*T^2 \tag{3}$$

This multiple linear regression results in an R^2 value of 0.95 with RMSE value of 0.15 when compared to the calibration data set of the NOAA OAP WCOA cruises from 2007 to 2016 (Feely and Sabine 2013; Feely et al. 2015, 2016*b,c*; Alin et al. 2017). Second, Ω_{ar} is also calculated using pCO_2 measured
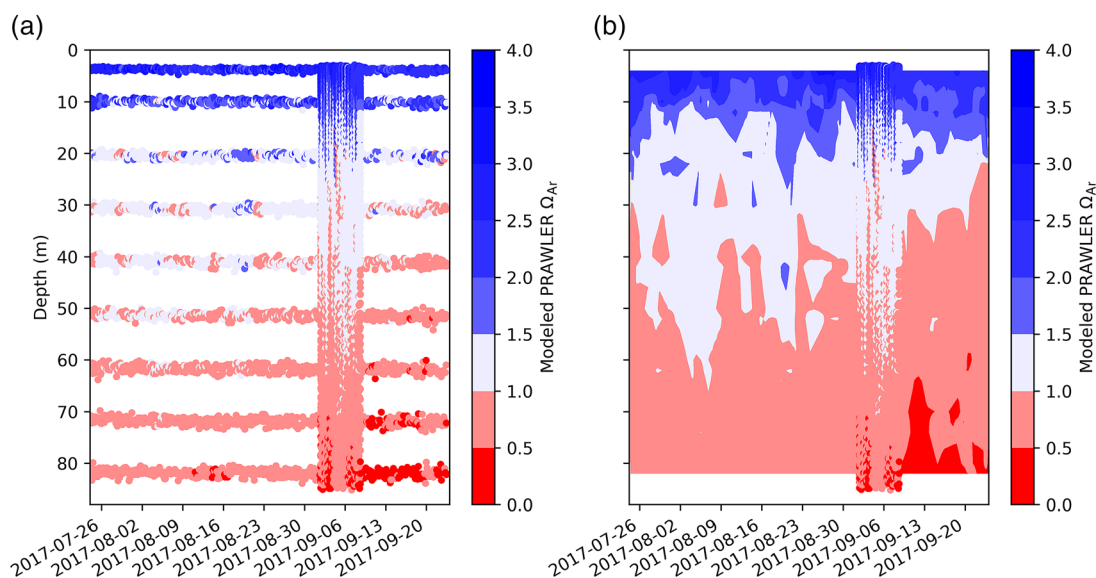
Fig. 8. (**a**) Algorithm-derived Ω_{ar} (Eq. 3) based on T, S, and O_2 measurements on the PRAWLER. (**b**) Contoured Ω_{ar} plots with filled intervals and the free-fall profiling data are overlaid.

from the optode and the empirical algorithm for TA from Eq. 2. Uncertainty is calculated for Ω_{ar} by propagating the respective uncertainties for $p\mathrm{CO}_2$ and TA through CO2SYS calculations applied to the whole data set (Orr et al. 2018). Using an average optode uncertainty from the three validation sets in Table 2 of 51 μatm, estimated Ω_{ar} uncertainty is 0.36 using Eq. 2 TA. Thus, the algorithm-based Ω_{ar} achieves lower uncertainty than the Ω_{ar} calculated using PRAWLER optode $p\mathrm{CO}_2$ and estimated TA, therefore the rest of this section will be presented using algorithm-based Ω_{ar} results.

Using the algorithm for direct calculation, Ω_{ar} ranged from close to 0 to ~ 4 (Fig. 8a,b). Ω_{ar} values > 1.5 were only seen in the surface waters shallower than 20 m depth. Below 60 m, undersaturation ($\Omega_{ar} < 1$) was observed throughout the deployment with periods where undersaturation extended to as shallow as 40 m. Extremely low $\Omega_{ar} < 0.5$ is found at 80 m depth in mid-September, coinciding with low O_2, high CO_2 seen previously (Figs. 3, 7). The NOAA OAP WCOA cruises (Feely et al. 2015, 2016*b,c*; Alin et al. 2017) sampled at various times between June and September of 2011 to 2013 and 2016. DIC and TA discrete samples were used in CO2SYS to calculate Ω_{ar} from the closest sampling stations from WCOA cruises (< 27 km away) resulting in undersaturated waters only seen below 80 m depth. From June 2016 at < 1 km away from the PRAWLER location, aragonite undersaturation started at ~ 83 m.

Discussion

Field evaluation of *p*CO₂ optode performance

To briefly summarize the optode performance in the field compared to our "gold standard" methods of Ćháʔba· MAPCO2™ and ASVCO2™ for surface data, the adjusted

PRAWLER optode $p\mathrm{CO}_2$ data have an average residual of 6 ± 42 μatm and 35 ± 31 μatm with RMSEs of 43 μatm and 46 μatm as well as 2% and 16% difference, respectively (Table 2). Using algorithm-estimated data to assess error throughout the water column, we see a slightly larger error and RMSE for optode data compared to the model of -28 ± 66 μatm, -6% difference, and RMSE of 72 μatm. Besides sensor error, spatial heterogeneity of water properties across sites contributes to the difference between PRAWLER optode and Ćháʔba· MAPCO2™ and ASVCO2™, while model uncertainty and on-shelf processes that can alter the fundamental relationships underlying the DIC model contribute to estimated error of the PRAWLER CO_2. In conclusion, the total uncertainty estimate based on the RMSEs for the $p\mathrm{CO}_2$ optode during the 2-month deployment on the PRAWLER of 43–72 μatm is likely conservative as it includes both sensor error and environmental variability between the PRAWLER and reference measurements.

Still, our results are comparable to the reported performance of the $p\mathrm{CO}_2$ optodes in previous studies, where observed accuracy varied within 2–75 μatm of the true value during deployments of 6–7 months in the dynamic coastal environment (Atamanchuk et al. 2015*a,b*). In these studies, optode measurements were compared to calculated $p\mathrm{CO}_2$ from DIC and TA water samples, with errors attributed to incomplete sensor conditioning, sensor drift, calculation, and water sampling. In another study, a $p\mathrm{CO}_2$ optode was deployed at a fixed depth side-by-side with an oxygen probe in Lake Ilmensee, Germany for 2 months in order to investigate lake metabolism (Peeters et al. 2016). The $p\mathrm{CO}_2$ data from the optode were compared against $p\mathrm{CO}_2$ data from a reference CO_2-IR probe (HydroC® CO_2, CONTROS) and were corrected for conditioning drift using the same methodology applied in

this study. Good agreement of the amplitude and the timing of the daily fluctuations in pCO$_2$ measured with the CO$_2$ optode and the CO$_2$-IR probe was found after the adjustment. On average, pCO$_2$ data had an error of -1 ± 12 μatm compared to CO$_2$-IR during a ~ 5 d period when both probes were deployed side-by-side. After application of the scaling factor to compensate for the initial conditioning drift, the pCO$_2$ optode provided reliable data over the duration of the study (Peeters et al. 2016). Better performance of the optode in the study of Peeters et al. (2016) can be attributed to the lack of dynamic errors introduced by profiling mode in this study and to the smaller range of pCO$_2$ values, where Peeters et al. (2016) covered a pCO$_2$ range of ~ 100 μatm and this study covers a range of ~ 2000 μatm. Additionally, the study by Peeters et al. (2016) was conducted in a lake with freshwater, so there were no salinity changes.

Comments and recommendations

The PRAWLER proved to be an effective test bed vehicle to use for our goal of evaluating prototype Aanderaa pCO$_2$ optode performance off the Washington coast. Its ability to transmit data in real time back to shore and allow for modifications to the sampling scheme were instrumental to this type of sensor assessment. Additionally, temperature and oxygen measured on the PRAWLER enabled us to estimate aragonite saturation with half the uncertainty than using the optode. In order to measure pCO$_2$ to weather- or climate-quality, target precision and accuracy would be 2.5% or 0.5%, respectively. A target response time would be similar or faster than available oxygen optodes, which ranges from 6 to 25 s (Bittig et al. 2014), in order to deploy the same sampling schemes and achieve the same resolution for the two parameters. The optode achieved an error uncertainty of 43–72 μatm based on RMSE (Table 2) during the 2-month deployment on the PRAWLER. It did not lose its calibration throughout the deployment despite the changing salinity (30.5–34) while profiling from 3 to 80 m. The equilibration time for the optode was longer than expected, taking > 18 min to fully equilibrate at 8°C, but was explained by the lack of sufficient flow against the sensing foil to promote faster diffusion. We were able to use a regional algorithm to make an adjustment to the drift in optode data. We acknowledge that not all optode deployments would have this available resource, where commonly, the only comparison points are discrete bottle samples taken during deployment and recovery. The optode captured changes in concentrations and recorded a high-CO$_2$ event toward the end of the deployment of a similar magnitude of change to that observed at the nearby MAPCO2™ on the Ćháʔba· mooring.

Suggestions to improve optode performance on future deployments involve more stable and sensitive sensing foils, reliable in situ calibration, and adding a pump to provide faster seawater flow rates against the sensor foil for faster

response times. Sensor drift should be monitored by comparing against reference data such as discrete bottle samples or the multiple checkpoints per day that we had planned to have using the instrument package below the mooring line. Future long-term profiling deployments would benefit from a more accurate instrument colocated with the optode that does not need to achieve the same measurement frequency (Peeters et al. 2016). Faster flow rates could be achieved by adding a pumped flow of water or a funnel could be attached to direct water to flow over the sensor foil which would increase the flow rate without requiring additional power. To allow the optode temperature to equilibrate faster and reduce the thermal mass, different housing materials could be used for the optode body. Additionally, for future deployments on the PRAWLER, surface waters may require longer soak times to allow the optode to equilibrate temperature and pCO$_2$, but shorter times could be used for deeper waters where temperature is more uniform. Faster equilibration and improved accuracy in pCO$_2$ optode measurements would provide high-frequency data that could be used to calculate calcium carbonate saturation states to provide further insights into dynamics of OA. These results could be incorporated into regional and global biogeochemical models to improve predictions of corrosive events.

References

Alford, M. H., J. B. Mickett, S. Zhang, P. MacCready, Z. Zhao, and J. Newton. 2012. Internal waves on the Washington continental shelf. Oceanography **25**: 66–79. doi:10.5670/oceanog.2012.43

Alin, S. R., R. A. Feely, A. G. Dickson, J. M. Hernández-Ayón, L. W. Juranek, M. D. Ohman, and R. Goericke. 2012. Robust empirical relationships for estimating the carbonate system in the southern California Current System and application to CalCOFI hydrographic cruise data (2005–2011). J. Geophys. Res. Oceans **117**: C05033. doi:10.1029/2011JC007511

Alin, S. R., R. A. Feely, B. Hales, R. H. Byrne, W. Cochlan, X. Liu, and D. Greeley. 2017. Dissolved inorganic carbon, total alkalinity, pH on total scale, and other variables collected from profile and discrete sample observations using CTD, Niskin bottle, and other instruments from NOAA Ship *Ronald H. Brown* in the U.S. West Coast California Current System from 2016-05-08 to 2016-06-06 (NCEI Accession 0169412). Version 1.1. NOAA National Centers for Environmental Information. Dataset. doi:10.7289/V5V40SHG

Atamanchuk, D., A. Tengberg, P. J. Thomas, J. Hovdenes, A. Apostolidis, C. Huber, and P. O. Hall. 2014. Performance of a lifetime-based optode for measuring partial pressure of carbon dioxide in natural waters. Limnol. Oceanogr.: Methods **12**: 63–73. doi:10.4319/lom.2014.12.63

Atamanchuk, D., M. Kononets, P. J. Thomas, J. Hovdenes, A. Tengberg, and P. O. J. Hall. 2015a. Continuous long-term observations of the carbonate system dynamics in the water column of a temperate fjord. J. Mar. Syst. **148**: 272–284. doi:10.1016/j.jmarsys.2015.03.002

Atamanchuk, D., A. Tengberg, D. Aleynik, P. Fietzek, K. Shitashima, A. Lichtschlag, P. O. Hall, and H. Stahl. 2015b. Detection of CO_2 leakage from a simulated sub-seabed storage site using three different types of pCO_2 sensors. Int. J. Greenh. Gas Control **38**: 121–134. doi:10.1016/j.ijggc.2014.10.021

Barton, A., B. Hales, G. G. Waldbusser, C. Langdon, and R. A. Feely. 2012. The Pacific oyster, *Crassostrea gigas*, shows negative correlation to naturally elevated carbon dioxide levels: Implications for near-term ocean acidification effects. Limnol. Oceanogr.: Methods **57**: 698–710. doi:10.4319/lo.2012.57.3.0698

Barton, A., and others. 2015. Impacts of coastal acidification on the Pacific Northwest shellfish industry and adaptation strategies implemented in response. Oceanography **28**: 146–159. doi:10.5670/oceanog.2015.38

Bauer, J. E., W. J. Cai, P. A. Raymond, T. S. Bianchi, C. S. Hopkinson, and P. A. G. Regnier. 2013. The changing carbon cycle of the coastal ocean. Nature **504**: 61–70. doi:10.1038/nature12857

Bednaršek, N., T. Klinger, C. J. Harvey, S. Weisberg, R. M. McCabe, R. A. Feely, J. Newton, and N. Tolimieri. 2017. New ocean, new needs: Application of pteropod shell dissolution as a biological indicator for marine resource management. Ecol. Indic. **76**: 240–244. doi:10.1016/j.ecolind.2017.01.025

Bittig, H. C., B. Fiedler, R. Scholz, G. Krahmann, and A. Körtzinger. 2014. Time response of oxygen optodes on profiling platforms and its dependence on flow speed and temperature. Limnol. Oceanogr.: Methods **12**: 617–636. doi:10.4319/lom.2014.12.617

Bittig, H. C., and others. 2018. Oxygen optode sensors: Principle, characterization, calibration, and application in the ocean. Front. Mar. Sci. **4**: 429. doi:10.3389/fmars.2017.00429

Bograd, S. J., C. G. Castro, E. Di Lorenzo, D. M. Palacios, H. Bailey, W. Gilly, and F. P. Chavez. 2008. Oxygen declines and the shoaling of the hypoxic boundary in the California Current. Geophys. Res. Lett. **35**: L12607. doi:10.1029/2008GL034185

Cai, W. J., and others. 2011. Acidification of subsurface coastal waters enhanced by eutrophication. Nat. Geosci. **4**: 766. doi:10.1038/ngeo1297

Caldeira, K., and M. E. Wickett. 2003. Anthropogenic carbon and ocean pH. Nature **425**: 365. doi:10.1038/425365a

Chan, F., J. A. Barth, J. Lubchenco, A. Kirincich, H. Weeks, W. T. Peterson, and B. A. Menge. 2008. Emergence of anoxia in the California current large marine ecosystem. Science **319**: 920. doi:10.1126/science.1149016

Connolly, T. P., B. M. Hickey, S. L. Geier, and W. P. Cochlan. 2010. Processes influencing seasonal hypoxia in the northern California Current System. J. Geophys. Res. Oceans **115**: C03021. doi:10.1029/2009JC005283

DeGrandpre, M. D., T. R. Hammar, S. P. Smith, and F. L. Sayles. 1995. In situ measurements of seawater pCO_2. Limnol. Oceanogr. **40**: 969–975. doi:10.4319/lo.1995.40.5.0969

Dickson, A. G. 1990a. Standard potential of the reaction: $AgCl(s) + 1/2H_2(g) = Ag(s) + HCl(aq)$, and the standard acidity constant of the ion HSO_4^- in synthetic sea water from 273.15 to 318.15 K. J. Chem. Thermodyn. **22**: 113–127. doi:10.1016/0021-9614(90)90074-Z

Dickson, A. G. 1990b. Thermodynamics of the dissociation of boric acid in synthetic seawater from 273.15 to 318.15 K. Deep-Sea Res. A **37**: 755–766. doi:10.1016/0198-0149(90)90004-F

Doney, S. C., V. J. Fabry, R. A. Feely, and J. A. Kleypas. 2009. Ocean acidification: The other CO_2 problem. Ann. Rev. Mar. Sci. **1**: 169–192. doi:10.1146/annurev.marine.010908.163834

Fassbender, A. J., C. L. Sabine, R. A. Feely, C. Langdon, and C. W. Mordy. 2011. Inorganic carbon dynamics during northern California coastal upwelling. Cont. Shelf Res. **31**: 1180–1192. doi:10.1016/j.csr.2011.04.006

Feely, R. A., C. L. Sabine, K. Lee, W. Berelson, J. Kleypas, V. J. Fabry, and F. J. Millero. 2004. Impact of anthropogenic CO_2 on the $CaCO_3$ system in the oceans. Science **305**: 362–366. doi:10.1126/science.1097329

Feely, R. A., C. L. Sabine, J. M. Hernandez-Ayon, D. Ianson, and B. Hales. 2008. Evidence for upwelling of corrosive "acidified" water onto the continental shelf. Science **320**: 1490–1492. doi:10.1126/science.1155676

Feely, R. A., and C. L. Sabine. 2013. Dissolved inorganic carbon, alkalinity, temperature, salinity and other variables collected from discrete sample and profile observations using Alkalinity titrator, CTD and other instruments from WECOMA in the U.S. West Coast California Current System from 2007-05-11 to 2007-06-14 (NCEI Accession 0083685) [accessed 2018 March 5]. NOAA National Centers for Environmental Information. Dataset. doi:10.3334/CDIAC/OTG.CLIVAR_NACP_WEST_COAST_CRUISE_2007

Feely, R. A., S. R. Alin, B. Hales, G. C. Johnson, R. H. Byrne, W. T. Peterson, X. Liu, and D. Greeley. 2015. Dissolved inorganic carbon, total alkalinity, pH and other variables collected from profile and discrete sample observations using CTD, Niskin bottle, and other instruments from NOAA Ship *Fairweather* and the R/V *Point Sur* in the U.S. West Coast California Current System during the 2013 West Coast Ocean Acidification Cruise (WCOA2013) from 2013-08-05 to 2013-08-28 (NCEI Accession 0132082). Version 3.3. NOAA National Centers for Environmental Information. Dataset. doi:10.7289/V5C53HXP

Feely, R. A., and others. 2016a. Chemical and biological impacts of ocean acidification along the west coast of North America. Estuar. Coast. Shelf Sci. **183**: 260–270. doi:10.1016/j.ecss.2016.08.043

Feely, R. A., and others. 2016b. Dissolved inorganic carbon, pH, alkalinity, temperature, salinity and other variables collected from discrete sample and profile observations using Alkalinity titrator, CTD and other instruments from WECOMA in the Gulf of the Farallones National Marine Sanctuary, Monterey Bay National Marine Sanctuary and others from 2011-08-12 to 2011-08-30 (NCEI Accession 0157458). Version 1.1. NOAA National Centers for Environmental Information. Dataset. Available from https://accession.nodc.noaa.gov/0157458

Feely, R. A., S. R. Alin, B. Hales, G. C. Johnson, L. W. Juranek, R. H. Byrne, W. T. Peterson, and D. Greeley. 2016c. Dissolved inorganic carbon, alkalinity, temperature, salinity and other variables collected from discrete sample and profile observations using Alkalinity titrator, CTD and other instruments from NOAA Ship *Bell M. Shimada* in the Columbia River estuary - Washington/Oregon, Gulf of the Farallones National Marine Sanctuary et al from 2012-09-04 to 2012-09-17 (NCEI Accession 0157445). Version 1.1 [accessed 2018 March 5]. NOAA National Centers for Environmental Information. Dataset. Available from https://accession.nodc.noaa.gov/0157445

Feely, R. A., R. R. Okazaki, W. J. Cai, N. Bednaršek, S. R. Alin, R. H. Byrne, and A. Fassbender. 2018. The combined effects of acidification and hypoxia on pH and aragonite saturation in the coastal waters of the California current ecosystem and the northern Gulf of Mexico. Cont. Shelf Res. **152**: 50–60. doi:10.1016/j.csr.2017.11.002

Harris, K. E., M. D. DeGrandpre, and B. Hales. 2013. Aragonite saturation state dynamics in a coastal upwelling zone. Geophys. Res. Lett. **40**: 2720–2725. doi:10.1002/grl.50460

Hickey, B. M., and N. S. Banas. 2008. Why is the northern end of the California Current System so productive? Oceanography **21**: 73–89. doi:10.5670/oceanog.2008.07

Hodgson, E. E., and others. 2018. Consequences of spatially variable ocean acidification in the California Current: Lower pH drives strongest declines in benthic species in southern regions while greatest economic impacts occur in northern regions. Ecol. Model. **383**: 106–117. doi:10.1016/j.ecolmodel.2018.05.018

Lewis, E., and D. W. R. Wallace. 1998. Program developed for CO_2 system calculations. ORNL/CDIAC-105. Carbon Dioxide Information Analysis Center, Oak Ridge National Laboratory. Available from https://salish-sea.pnnl.gov/media/ORNL-CDIAC-105.pdf

Lueker, T. J., A. G. Dickson, and C. D. Keeling. 2000. Ocean pCO_2 calculated from dissolved inorganic carbon, alkalinity, and equations for K1 and K2: Validation based on laboratory measurements of CO_2 in gas and seawater at equilibrium. Mar. Chem. **70**: 105–119. doi:10.1016/S0304-4203(00)00022-0

Martz, T. R., J. G. Connery, and K. S. Johnson. 2010. Testing the Honeywell Durafet® for seawater pH applications. Limnol. Oceanogr.: Methods **8**: 172–184. doi:10.4319/lom.2010.8.172

Martz, T. R., K. Daly, R. H. Byrne, J. Stillman, and D. Turk. 2015. Technology for ocean acidification research: Needs and availability. Oceanography **25**: 40–47. doi:10.5670/oceanog.2015.30

McNeil, B. I., and T. P. Sasse. 2016. Future ocean hypercapnia driven by anthropogenic amplification of the natural CO_2 cycle. Nature **529**: 383–386. doi:10.1038/nature16156

Millero, F. J. 1995. Thermodynamics of the carbon dioxide system in the oceans. Geochim. Cosmochim. Acta **59**: 661–677. doi:10.1016/0016-7037(94)00354-O

Nam, S., H.-J. Kim, and U. Send. 2011. Amplification of hypoxic and acidic events by La Niña conditions on the continental shelf off California. Geophys. Res. Lett. **38**: L22602. doi:10.1029/2011GL049549

Newton, J. A., R. A. Feely, E. B. Jewett, P. Williamson, and J. Mathis. 2015. Global ocean acidification observing network: Requirements and governance plan. GOA-ON: 2nd ed. doi:10.4314/ahs.v15i3.5

Orr, J. C., and others. 2005. Anthropogenic ocean acidification over the twenty-first century and its impact on calcifying organisms. Nature **437**: 681. doi:10.1038/nature04095

Orr, J. C., J. M. Epitalon, A. G. Dickson, and J. P. Gattuso. 2018. Routine uncertainty propagation for the marine carbon dioxide system. Mar. Chem. **207**: 84–107. doi:10.1016/j.marchem.2018.10.006

Osse, J., S. Stalin, C. Meinig, and H. Milburn. 2015. The PRAWLER, a vertical profiler: Powered by wave energy. *In* Oceans 2015 MTS/IEEE, 19–22 October 2015. Marine Technology Society and Institute of Electrical and Electronic Engineers. doi:10.23919/OCEANS.2015.7404354

Peeters, F., D. Atamanchuk, A. Tengberg, J. Encinas-Fernandez, and H. Hofmann. 2016. Lake metabolism: Comparison of lake metabolic rates estimated from a diel CO_{2-} and the common diel O_{2-} technique. PLoS One **11**: e0168393. doi:10.1371/journal.pone.0168393

PSEMP Marine Waters Workgroup. 2017. Puget Sound marine waters: 2016 overview. S. K. Moore, R. Wold, K. Stark, J. Bos, P. Williams, N. Hamel, A. Edwards, C. Krembs, and J. Newton, editors.

Reum, J. C. P., and others. 2015. Interpretation and design of ocean acidification experiments in upwelling systems in the context of carbonate chemistry co-variation with temperature and oxygen. ICES J. Mar. Sci. **73**: 582–595. doi:10.1093/icesjms/fsu231

Seidel, M. P., M. D. DeGrandpre, and A. G. Dickson. 2008. A sensor for in situ indicator-based measurements of seawater pH. Mar. Chem. **109**: 18–28. doi:10.1016/j.marchem.2007.11.013

Siedlecki, S. A., N. S. Banas, K. A. Davis, S. Giddings, B. M. Hickey, P. MacCready, T. Connolly, and S. Geier. 2015. Seasonal and interannual oxygen variability on the Washington and Oregon continental shelves. J. Geophys. Res. Oceans **120**: 608–633. doi:10.1002/2014JC010254

Siedlecki, S. A., and others. 2016. Experiments with seasonal forecasts of ocean conditions for the Northern region of the California Current upwelling system. Sci. Rep. **6**: 27203. doi:10.1038/srep27203

Sutton, A. J., and others. 2014. A high-frequency atmospheric and seawater pCO_2 data set from 14 open-ocean sites using a moored autonomous system. Earth Syst. Sci. Data **6**: 353–366. doi:10.5194/essd-6-353-2014

Sutton, A. J., and others. 2016. Using present-day observations to detect when anthropogenic change forces surface ocean carbonate chemistry outside preindustrial bounds. Biogeosciences **13**: 5065–5083. doi:10.5194/bg-13-5065-2016

Uppstrom, L. R. 1974. The boron-chlorinity ratio of deep seawater from the Pacific Ocean. Deep-Sea Res. Part I Oceanogr. Res. Pap. **21**: 161–162. doi:10.1016/0011-7471(74)90074-6

van Heuven, S., D. Pierrot, J. W. B. Rae, E. Lewis, and D. W. R. Wallace. 2011. MATLAB program developed for CO_2 system calculations. ORNL/CDIAC-105b. Carbon Dioxide Information Analysis Center, Oak Ridge National Laboratory, U.S. Department of Energy. doi:10.3334/CDIAC/otg.CO2SYS_MATLAB_v1.1

Wallace, R. B., H. Baumann, J. S. Grear, R. C. Aller, and C. J. Gobler. 2014. Coastal ocean acidification: The other eutrophication problem. Estuar. Coast. Shelf Sci. **148**: 1–13. doi:10.1016/j.ecss.2014.05.027

Conflict of Interest

None declared.